LA-UR-14-29051
Approved for public release; distribution is unlimited.

Title: Demonstration of On-the-Fly Generation of Unresolved Resonance Region Cross Sections in a Monte Carlo Transport Code

Author(s): Walsh, Jonathan A.
Kiedrowski, Brian Christopher
Forget, Benoit
Smith, Kord S.
Brown, Forrest B.

Intended for: Monte Carlo R&D documentation

Issued: 2014-11-21

Demonstration of On-the-Fly Generation of Unresolved Resonance Region Cross Sections in a Monte Carlo Transport Code

Jonathan A. Walsh[1], Brian C. Kiedrowski[2], Benoit Forget[1], Kord S. Smith[1], and Forrest B. Brown[2]

[1]Department of Nuclear Science and Engineering
Massachusetts Institute of Technology
Cambridge, MA

[2]XCP-3, Monte Carlo Codes
Los Alamos National Laboratory
Los Alamos, NM

November 4, 2014

Abstract

In this preliminary investigation we demonstrate on-the-fly computation of unresolved resonance region cross sections. The on-the-fly method is implemented and tested in the OpenMC Monte Carlo neutron transport code. Preliminary results indicate that, in simulations of a system that is known to be highly sensitive to the effects of resonance structure in unresolved region cross sections, the on-the-fly treatment produces results that are in excellent agreement with those produced with the well-established probability table method. Additionally, we use the on-the-fly approach to show that accounting for the resonance structure of the competitive inelastic scattering reaction cross section can have non-negligible effects for an intermediate spectrum system. Comparisons between differential reaction rates and k_{eff} eigenvalues obtained using infinite-dilute, probability table, and on-the-fly cross sections in simulations of the Big Ten critical assembly are presented in this initial study.

1 Introduction

In this section we give brief introductions to important physical phenomena that characterize the unresolved resonance energy region and the computational methods that have typically been employed for capturing the effects of those phenomena in Monte Carlo simulations. Section 1.1 highlights defining characteristics of the unresolved resonance region as applicable to neutron transport simulations. In Section 1.2 we describe the use of so-called infinite-dilute cross sections in the unresolved resonance region and the pitfalls of this approach. The probability table method for treating resonance cross section structure in the unresolved region is outlined in Section 1.3. In Section 2 we explain the on-the-fly method of generating cross sections in the unresolved resonance region. Initial results obtained with the on-the-fly method are presented in Section 3 along with results obtained with the infinite-dilute and probability table methods. Preliminary conclusions reached in this initial study and areas for future research are discussed in Section 4.

1.1 Unresolved Resonance Region

At sufficiently high incident neutron energies, on average, individual resonances become broader, exhibit lower peak values, and are spaced close enough together that they overlap significantly with one another. In this region, the localized structure of a single resonance is insignificant relative to the collective structure of several resonances spanning a wider energy range. The energies that are characterized by this sort of cross section behavior comprise the fast energy region [5]. The fast energy region boundaries for different nuclides will vary with the onset coming at lower energies for heavier nuclides than for lighter ones. At somewhat lower incident neutron energies, the resonances for a given nuclide will be narrower, more pronounced, and better separated from neighboring resonances. These properties make individual resonances more easily distinguishable from one another in cross section measurement experiments. That is, the resonances can be resolved experimentally. Unlike in the fast energy region, there is sharp structure associated with individual resonances at these energies and this structure must be carefully accounted for in neutron transport simulations. Energies characterized by this type of behavior make up the resolved resonance region [5]. The intermediate incident neutron energies between the resolved resonance and fast energy regions make up the unresolved resonance region (URR). In the URR, individual resonances cannot all be resolved experimentally even though, in physical reality, each resonance exhibits distinct structure, just as in the resolved resonance region. As a result, precise cross section values are

unknown in the URR. Instead of precise descriptions of URR resonances and cross sections, we must rely on average descriptions and statistical distributions [5].

1.2 Infinite-Dilute Cross Sections

A precisely known cross section value for reaction x can be written as a Lebesgue integral in terms of a Dirac δ-function in σ'_x-space such that

$$\sigma_x(E_n) = \int_{-\infty}^{\infty} d\sigma'_x \delta(\sigma'_x - \sigma_x(E_n))\sigma'_x. \tag{1}$$

This is, though, just a special instance of a more general case in which we cannot collapse the distribution of σ'_x values to a precise value with a δ-function. However, we can write an expression for the expected cross section value,

$$\langle \sigma_x(E_n) \rangle = \int_{-\infty}^{\infty} d\sigma'_x P(\sigma'_x|E_n)\sigma'_x, \tag{2}$$

which is commonly referred to as an infinite-dilute cross section, $\sigma_x^{\infty}(E_n)$. This is the situation we are faced with when dealing with URR cross sections. We do not know precise values, but, based on mean unresolved resonance parameter values and the statistical distributions of those values, we can reconstruct the distribution, $P(\sigma'_x|E_n)$, of cross section values at a given neutron energy. Knowing this distribution then allows us to compute the expected, infinite-dilute values. Historically, in the absence of precisely known URR resonance structure, these infinite-dilute cross sections were used in Monte Carlo neutron transport simulations.

Use of the infinite-dilute cross sections, though, is tantamount to neglecting energy self-shielding effects. By obtaining expected cross section values in the manner just described, we have smoothed out the resonance structure of the URR. That is, in the narrow energy intervals where resonances actually occur, we have a reduced value, and in the wider energy intervals between real URR resonances, we have an increased value. So, over the majority of URR energies, infinite-dilute cross sections are greater than the unknown, precise values. It is known that this phenomenon leads to significant over-predictions of capture by resonant absorbers (e.g. ^{238}U) in intermediate energy spectrum systems when infinite-dilute cross sections are used in simulations. This results in under-predicted, non-conservative k_{eff} eigenvalue calculations [12].

1.3 Probability Tables

In order to more faithfully account for resonance structure and the resulting self-shielding effects in the URR - phenomena that can be worth hundreds of pcm in intermediate spectrum systems - the probability table method was proposed [8]. This method relies on the sampling of discrete cross section values with associated discrete probabilities such that, in the limit of many samples, the expected cross section value at a given E_n is preserved. Although expected cross sections are preserved, the distribution of discrete cross section-probability pairs provides a more realistic model for URR self-shielding effects. Certain practical considerations in implementing the probability table method are well-documented [15][4][9].

2 On-the-Fly Cross Section Generation

In this section we describe the on-the-fly method of generating URR cross sections, as implemented in OpenMC. The sampling of unresolved resonance parameters and use of the sampled parameters in cross section computations using the single-level Breit-Wigner formulae are discussed in Sections 2.1 and 2.2, respectively. Where possible, we use variables that are consistent in notation with those in the ENDF-6 Formats Manual [18].

2.1 Level Spacings and Partial Widths

In the energy region about any incident neutron laboratory system energy, E_n, at which we wish to compute a realization of URR cross section values, we must statistically generate an ensemble of resonances. This ensemble, sometimes referred to as a resonance ladder, is determined by the energies at which resonances occur as well as the partial reaction widths characterizing each of the resonances. The process for sampling these values proceeds directly from the unresolved resonance parameters given in File 2 of an ENDF-6 file.

We are first concerned with the energy-dependent mean unresolved resonance parameter values given for an individual spin sequence which is defined by an orbital angular momentum quantum number, l, and a total angular momentum quantum number, J_j. There are NLS orbital quantum numbers associated with the URR for a given nuclide. For each of these NLS values, there are NJS_l total angular momentum quantum numbers. That is, NLS is a nuclide-dependent quantity and NJS_l is dependent on both the nuclide and the l values for that nuclide.

For each $l - J_j$ spin sequence, we sample level spacings (i.e. energy differences between adjacent resonance energies) and partial reaction widths using those parameters' mean values and their statistical distributions. The mean parameter values at a specific E_n are determined by interpolation between the values at the energies tabulated in the ENDF-6 File 2[1]. The spread of level spacing and partial reaction width values can be described by the Wigner distribution and χ^2 distributions with varying degrees of freedom, respectively. Table 1 gives level spacing and partial width variable notation and Table 2 gives the notation that will be used for the degrees of freedom for each of the partial width χ^2 distributions.

The Wigner distribution for level spacings is given by

$$P_W\left(\frac{D_{l,J_j}}{\langle D_{l,J_j}(E_n)\rangle}\right) = \frac{\pi D_{l,J_j}}{2\langle D_{l,J_j}(E_n)\rangle}\exp\left(-\frac{\pi D_{l,J_j}^2}{4\langle D_{l,J_j}(E_n)\rangle^2}\right). \tag{3}$$

Direct sampling of this distribution gives

$$D_{l,J_j} = \langle D_{l,J_j}(E_n)\rangle\sqrt{-4\log(\xi)/\pi}, \tag{4}$$

for a random number on the unit interval, ξ.

Partial widths for reaction $*$, G^*, are obtained by sampling a χ^2 distribution with the appropriate variables for the number of degrees of freedom, AMU^*, as given in Table 2. Therefore, we sample

$$\begin{aligned} &P_{\chi^2_{AMU^*}}\left(AMU^*\frac{G^*_{l,J_j}}{\langle G^*_{l,J_j}(E_n)\rangle}\right) \\ &\quad = \frac{\exp\left(-\frac{AMU^*}{2}\frac{G^*_{l,J_j}}{\langle G^*_{l,J_j}(E_n)\rangle}\right)}{2^{AMU^*/2}\Gamma\left(\frac{AMU^*}{2}\right)}\left(AMU^*\frac{G^*_{l,J_j}}{\langle G^*_{l,J_j}(E_n)\rangle}\right)^{\frac{AMU^*}{2}-1} \end{aligned} \tag{5}$$

and then calculate the sampled widths as

$$GN_{l,J_j} = \nu\sqrt{E_\lambda}\frac{\langle GN0_{l,J_j}(E_n)\rangle}{AMUN_{l,J_j}}\frac{GN0_{l,J_j}}{\langle GN0_{l,J_j}(E_n)\rangle}, \tag{6}$$

$$GG_{l,J_j} = \langle GG_{l,J_j}(E_n)\rangle, \tag{7}$$

$$GF_{l,J_j} = \frac{\langle GF_{l,J_j}(E_n)\rangle}{AMUF_{l,J_j}}\frac{GF_{l,J_j}}{\langle GF_{l,J_j}(E_n)\rangle}, \tag{8}$$

[1]The nuclide-dependent interpolation scheme is prescribed in the ENDF-6 file.

and

$$GX_{l,J_j} = \frac{\langle GX_{l,J_j}(E_n)\rangle}{AMUX_{l,J_j}} \frac{GX_{l,J_j}}{\langle GX_{l,J_j}(E_n)\rangle}. \tag{9}$$

The $\Gamma\left(\frac{AMU^*}{2}\right)$ term in Eq. 5 is the mathematical Gamma function. The derived variables ρ and ν are given by $ak(E_\lambda)$ and P_l/ρ, respectively. In these expressions, a, $k(E_\lambda)$, and P_l are the channel radius, center-of-mass neutron wavenumber at a resonance energy, E_λ, and orbital quantum number-dependent penetration factor, respectively. The wavenumber is given by

$$k(E) = \frac{10\sqrt{2m_n}}{\hbar c} \frac{AWR}{AWR+1} \sqrt{E}. \tag{10}$$

with m_n, $\hbar c$, and AWR being the mass of a neutron in eV, the reduced Planck constant multiplied by the speed of light in eV-fm, and the ratio of the mass of the target nuclide to that of a neutron, respectively. The channel radius is related to the scattering radius, AP, which is to be treated as energy-dependent, or not, if the NRO ENDF flag is 1 or 0, respectively. For a scattering radius that is independent of energy, a $NAPS$ ENDF flag set to 0 indicates that the channel radius should be calculated as

$$a = 0.123 \times AWR^{1/3} + 0.08. \tag{11}$$

In this case, a should be used in the computation of penetrabilities, P_l, and shift factors, S_l, whereas AP should be used to calculate hard sphere phase shifts, ϕ_l. If the $NAPS$ flag is set to 1, AP should be used in determining the penetrabilities, shift factors, and phase shifts.

For a scattering radius that is dependent on energy, as in the energy-independent case, $NAPS$ set to 0 indicates that a is to be computed with Eq. 11 and used in the penetrabilities and shift factors with AP being used in the hard sphere phase shifts. If $NAPS$ is set to 1 or 2, the penetrabilities, shift factors, and phase shifts are all calculated using AP. However, in the case that $NAPS$ is set to 2, an energy-independent AP is given and should be used for P_l and S_l. Expressions for P_l and S_l are given in the next section.

2.2 Single-Level Breit-Wigner Cross Sections

Cross section values at a given E_n are computed using a so-called "many-level Breit-Wigner" model[2] [6]. In this model, the cross section values at E_n are

[2]This many-level Breit-Wigner model should not be confused with the multi-level Breit-Wigner (MLBW) resonance formalism.

Variable	Symbol
Mean Level Spacing	$\langle D_{l,J_j}(E_n)\rangle$
Sampled Level Spacing	D_{l,J_j}
Mean Reduced Neutron Width	$\langle GN0_{l,J_j}(E_n)\rangle$
Sampled Neutron Width	GN_{l,J_j}
Mean Radiative Capture Width	$\langle GG_{l,J_j}(E_n)\rangle$
Sampled Radiative Capture Width	GG_{l,J_j}
Mean Fission Width	$\langle GF_{l,J_j}(E_n)\rangle$
Sampled Fission Width	GF_{l,J_j}
Mean Competitive Reaction Width	$\langle GX_{l,J_j}(E_n)\rangle$
Sampled Competitive Reaction Width	GX_{l,J_j}

Table 1: Unresolved Resonance Parameter Variables

Variable	Symbol
Neutron Width DOF	$AMUN_{l,J_j}$
Radiative Capture Width DOF	$AMUG_{l,J_j}$
Fission Width DOF	$AMUF_{l,J_j}$
Competitive Reaction Width DOF	$AMUX_{l,J_j}$

Table 2: Partial Width χ^2 Distribution Variables

computed as a summation of the contributions from each of N_{res} resonances at this energy. The value of N_{res} must be chosen to be high enough that the addition of a nominal resonance's contribution to the cross section values at E_n is negligible.

The SLBW elastic neutron scattering cross section is given by

$$\begin{aligned}\sigma_n(E_n) &= \sigma_{\text{pot}}(E_n) \\ &+ \Sigma_{l=0}^{NLS-1}\Sigma_{j=1}^{NJS_l}\Sigma_{\lambda=1}^{N_{\text{res}}} \\ &\sigma_\lambda\left(\left[\cos\left(2\phi_l(\rho)\right) - \left(1 - \frac{\Gamma_{n,\lambda}}{\Gamma_\lambda}\right)\right]\psi(\theta,x) + \chi(\theta,x)\sin\left(2\phi_l(\rho)\right)\right).\end{aligned} \tag{12}$$

The potential, or shape elastic, scattering cross section appears in the above expression and is calculated as

$$\sigma_{\text{pot}}(E_n) = \frac{4\pi}{k(E_n)^2}\Sigma_{l=0}^{NLS-1}(2l+1)\sin^2\left(\phi_l(\rho)\right). \tag{13}$$

Radiative capture, fission, and competitive inelastic scattering cross sections are given by

$$\sigma_\gamma(E_n) = \Sigma_{l=0}^{NLS-1}\Sigma_{j=1}^{NJS_l}\Sigma_{\lambda=1}^{N_{\text{res}}}\sigma_\lambda\frac{\Gamma_{\gamma,\lambda}}{\Gamma_\lambda}\psi(\theta,x), \tag{14}$$

$$\sigma_f(E_n) = \Sigma_{l=0}^{NLS-1}\Sigma_{j=1}^{NJS_l}\Sigma_{\lambda=1}^{N_{\text{res}}}\sigma_\lambda\frac{\Gamma_{f,\lambda}}{\Gamma_\lambda}\psi(\theta,x), \tag{15}$$

and

$$\sigma_x(E_n) = \Sigma_{l=0}^{NLS-1}\Sigma_{j=1}^{NJS_l}\Sigma_{\lambda=1}^{N_{\text{res}}}\sigma_\lambda\frac{\Gamma_{x,\lambda}}{\Gamma_\lambda}\psi(\theta,x), \tag{16}$$

respectively. The total cross section is calculated as the sum of the partials,

$$\sigma_{\text{tot}}(E_n) = \sigma_n(E_n) + \sigma_\gamma(E_n) + \sigma_f(E_n) + \sigma_x(E_n). \tag{17}$$

Other variables needed for the computation of cross sections include the resonance peak value,

$$\sigma_\lambda = g_{J_j}\frac{4\pi}{k(E_\lambda)^2}\frac{GN_{l,J_j}}{GT_{l,J_j}}, \tag{18}$$

the statistical spin factor,

$$g_{J_j} = \frac{2J_j+1}{4SPI+2}, \tag{19}$$

the energy-dependent neutron width,

$$\Gamma_{n,\lambda} = \frac{GN_{l,J_j}P_l(\rho_n)}{P_l(\rho_\lambda)}, \tag{20}$$

$$\theta = \frac{\Gamma_\lambda}{2\sqrt{k_{\mathrm{B}}TE_n/AWR}}, \tag{21}$$

with T being the temperature of the material in which the target nuclide resides,

$$x = \frac{2(E_n - E'_\lambda)}{\Gamma_\lambda}, \tag{22}$$

and the shifted resonance energy,

$$E'_\lambda = E_\lambda + \frac{GN_{l,J_j}(S_l(\rho_\lambda) - S_l(\rho_n))}{2P_l(\rho_\lambda)}. \tag{23}$$

The penetrabilities, hard sphere phase shifts, and resonance energy shift factors are given by

$$P_l(\rho) = \begin{cases} \rho & l = 0 \\ \frac{\rho^3}{1+\rho^2} & l = 1 \\ \frac{\rho^5}{9+3\rho^2+\rho^4} & l = 2 \\ \frac{\rho^7}{225+45\rho^2+6\rho^4+\rho^6} & l = 3 \\ \frac{\rho^9}{11025+1575\rho^2+135\rho^4+10\rho^6+\rho^8} & l = 4, \end{cases} \tag{24}$$

$$\phi_l(\rho) = \begin{cases} \rho & l = 0 \\ \rho - \tan^{-1}(\rho) & l = 1 \\ \rho - \tan^{-1}\left(\frac{3\rho}{3-\rho^2}\right) & l = 2 \\ \rho - \tan^{-1}\left(\frac{15\rho-\rho^3}{15-6\rho^2}\right) & l = 3 \\ \rho - \tan^{-1}\left(\frac{105\rho-10\rho^3}{105-45\rho^2+\rho^4}\right) & l = 4, \end{cases} \tag{25}$$

and

$$S_l(\rho) = \begin{cases} 0 & l = 0 \\ -\frac{1}{1+\rho^2} & l = 1 \\ -\frac{18+3\rho^2}{9+3\rho^2+\rho^4} & l = 2 \\ -\frac{675+90\rho^2+6\rho^4}{225+45\rho^2+6\rho^4+\rho^6} & l = 3 \\ -\frac{44100+4725\rho^2+270\rho^4+10\rho^6}{11025+1575\rho^2+135\rho^4+10\rho^6+\rho^8} & l = 4, \end{cases} \tag{26}$$

respectively.

Continuous-energy Doppler broadening - as opposed to the point-wise kernel broadening of the SIGMA1 method [3] - is accomplished using the ψ and χ Doppler integral functions [1]. These functions are given by

$$\psi(\theta, x) = \frac{\theta\sqrt{\pi}}{2}\mathrm{Re}\left[W\left(\frac{\theta x}{2}, \frac{\theta}{2}\right)\right] \tag{27}$$

and

$$\chi(\theta, x) = \frac{\theta\sqrt{\pi}}{2}\mathrm{Im}\left[W\left(\frac{\theta x}{2}, \frac{\theta}{2}\right)\right], \tag{28}$$

respectively. The W-function, also known as the Faddeeva function, is defined as

$$W(\alpha, \beta) = \exp\left(-z^2\right)\mathrm{erfc}\left(-iz\right) = \frac{i}{\pi}\int_{-\infty}^{\infty} dt \frac{\exp\left(-t^2\right)}{z - t} \tag{29}$$

with α and β being the real and imaginary components, respectively, of complex number $z = \alpha + i\beta$.

3 Initial Results

In this section we present results obtained from OpenMC simulations of the Big Ten critical assembly [7]. The particular model of the system is taken from the International Criticality Safety Benchmark Evaluation Project (ICSBEP) collection [13]. In Section 3.1 we present effective multiplication factor, k_{eff}, eigenvalue results and in Section 3.2 we examine differential absorption rates. Multiple URR cross section treatments are considered.

All simulations are performed using the ENDF70 neutron data library [16]. This library contains ENDF/B-VII.0 nuclear data [2] processed into ACE format with the NJOY Nuclear Data Processing System [10].

3.1 k_{eff} Eigenvalues and Integral Absorption Rates

Tables 3 and 4 give the effective multiplication factors and integral URR ^{238}U absorption rates, respectively, for different unresolved region cross section treatments. We see that accounting for the resonance structure of ^{238}U cross sections, with either probability tables or on-the-fly calculations, results in a $\sim$ 400 pcm increase in k_{eff} relative to the case in which infinite-dilute cross sections are utilized. Modeling the resonance structure of the first level inelastic scattering reaction cross section contributes another $\sim$ 40 pcm increase. Corresponding effects are seen in URR absorption rates.

^{238}U XS	Other Nuclides	Inelastic XS	k_{eff}	$1\sigma_{\text{mean}}$
Infinite-Dilute	Infinite-Dilute	Infinite-Dilute	1.00098	0.00010
Prob. Tables	Prob. Tables	Infinite-Dilute	1.00490	0.00009
OTF	Prob. Tables	Infinite-Dilute	1.00485	0.00010
OTF	Prob. Tables	Self-Shielded	1.00528	0.00009

Table 3: Comparison of k_{eff} for Various URR Treatments

^{238}U XS	Other Nuclides	Inelastic XS	Abs. Rate	$1\sigma_{\text{mean}}$
Infinite-Dilute	Infinite-Dilute	Infinite-Dilute	0.23014	0.00007
Prob. Tables	Prob. Tables	Infinite-Dilute	0.22329	0.00007
OTF	Prob. Tables	Infinite-Dilute	0.22340	0.00006
OTF	Prob. Tables	Self-Shielded	0.22548	0.00006

Table 4: ^{238}U URR Absorption Rates for Various URR Treatments

3.2 Differential Absorption Rates

Figures 1a and 1b show the ^{238}U absorption rates over the entire energy spectrum and in the URR, respectively, for both probability table and on-the-fly cross section treatments. Very good agreement is observed between the differential results produced with the two methods. For a consistent comparison, here, infinite-dilute inelastic scattering cross sections are used in both cases.

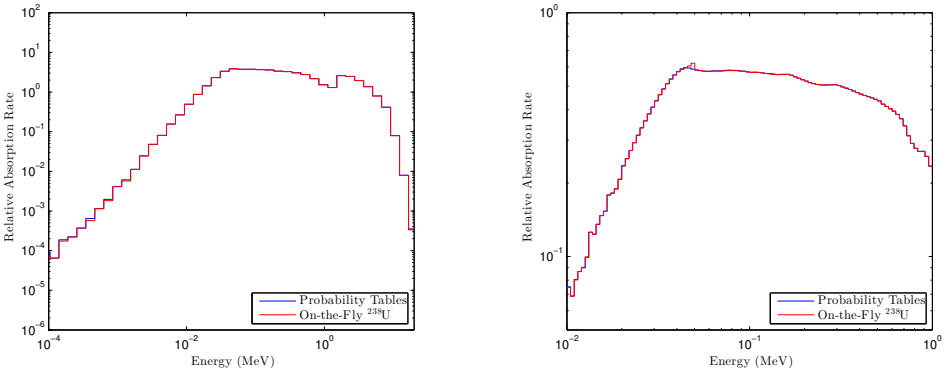

(a) Entire Spectrum (b) URR

Figure 1: Absorption with Probability Tables and OTF Computations

3.3 Self-Shielded Inelastic Scattering Cross Sections

The ENDF-6 format prescribes the use of the ENDF File 3 infinite-dilute cross section values for the competitive inelastic scattering reaction in the URR [18]. In Table 3, we see a $\sim$ 40 pcm increase in k_{eff} when the resonance structure of the ^{238}U first level inelastic scattering cross section is accounted for relative to the case in which the infinite-dilute values are used. Using the commonly employed 95% confidence interval as an acceptance criterion, this difference lies outside of statistical uncertainties. The possibility of different treatments of the competitive inelastic scattering cross section inducing differences in simulation results is mentioned by MacFarlane, et. al [11]. In their code-to-code comparison study of Big Ten critical assembly simulation results, it is noted that the TRIPOLI code [17], in making use of URR cross section data generated with the CALENDF data processing code [14], accounts for the resonance structure of the inelastic scattering cross section. Many other transport codes, such as MCNP [19], utilize the infinite-dilute URR cross section values that are produced by the NJOY processing code. Here, in OpenMC, we have isolated inelastic scattering cross section resonance structure effects by allowing for the on-the-fly use of either infinite-dilute or shielded values.

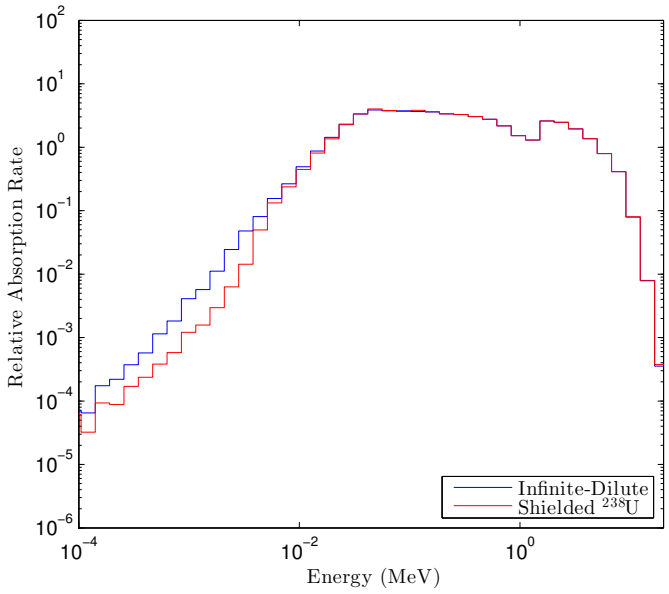

Figure 2: Inelastic Scattering Cross Section Absorption Rate Effects

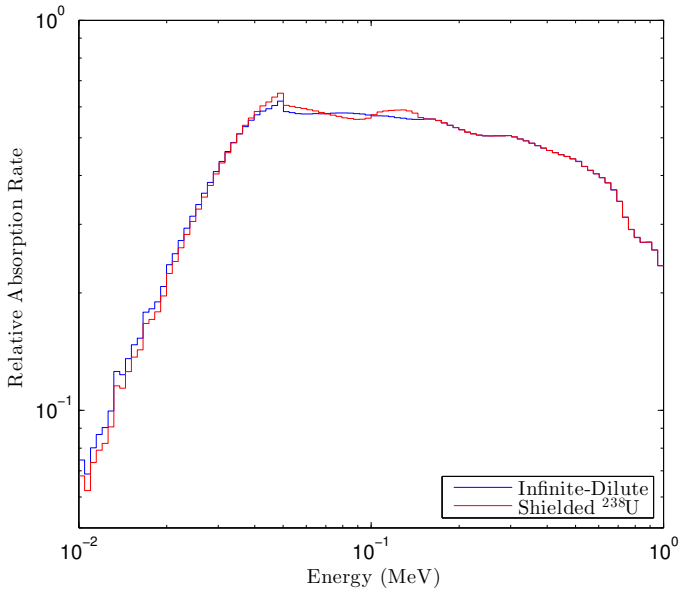

Figure 3: URR Inelastic Scattering Cross Section Absorption Rate Effects

4 Conclusions and Future Work

The work presented in this initial report demonstrates a procedure for computing URR cross sections on-the-fly in Monte Carlo neutron transport codes. Excellent agreement is observed in comparisons of integral and differential absorption rates, as well k_{eff} eigenvalues, that are calculated using the on-the-fly method with those obtained using probability tables. This agreement is achieved in simulations of the Big Ten critical assembly which is an intermediate spectrum system that is highly sensitive to URR resonance effects.

Computation of URR cross sections on-the-fly in the course of a simulation can be computationally expensive with respect to runtime. Quantification of these costs is necessary in order to establish the method's practical viability. Because on-the-fly computations rely on unresolved resonance parameters rather than probability tables of arbitrary size, memory reduction is typically achieved with the method. These reductions should also be quantified. The on-the-fly method is only applied to ^{238}U in these studies. Extending the application of the method to other nuclides should be investigated. The impact of an extended application on both calculated results and computational efficiency will be of interest in these investigations.

References

[1] G. I. Bell and S. Glasstone. *Nuclear Reactor Theory*. Division of Technical Information, United States Atomic Energy Commission, 1970.

[2] M. Chadwick, P. Obložinský, M. Herman, N. Greene, R. McKnight, D. Smith, P. Young, R. MacFarlane, G. Hale, S. Frankle, A. Kahler, T. Kawano, R. Little, D. Madland, P. Moller, R. Mosteller, P. Page, P. Talou, H. Trellue, M. White, W. Wilson, R. Arcilla, C. Dunford, S. Mughabghab, B. Pritychenko, D. Rochman, A. Sonzogni, C. Lubitz, T. Trumbull, J. Weinman, D. Brown, D. Cullen, D. Heinrichs, D. McNabb, H. Derrien, M. Dunn, N. Larson, L. Leal, A. Carlson, R. Block, J. Briggs, E. Cheng, H. Huria, M. Zerkle, K. Kozier, A. Courcelle, V. Pronyaev, and S. van der Marck. ENDF/B-VII.0: next generation evaluated nuclear data library for nuclear science and technology. *Nuclear Data Sheets*, 107:2931–3060, 2006.

[3] D. Cullen and C. Weisbin. Exact Doppler broadening of tabulated cross sections. *Nuclear Science and Engineering*, 60.3:199–229, 1976.

[4] M. Dunn and L. Leal. Calculating probability tables for the unresolved-resonance region using Monte Carlo methods. *Nuclear Science and Engineering*, 148:30–42, 2004.

[5] A. Foderaro. *The Elements of Neutron Interaction Theory*. MIT Press, 1971.

[6] F. Fröhner. Applied neutron resonance theory. Technical Report KfK 2669, Institute for Neutron Physics and Reactor Technology, Karlsruhe Nuclear Research Center, 1978.

[7] G. Hansen and H. Paxton. A critical assembly of uranium enriched to 10% in uranium-235. *Nuclear Science and Engineering*, 72:230–236, 1979.

[8] L. Levitt. The probability table method for treating unresolved neutron resonances in Monte Carlo calculations. *Nuclear Science and Engineering*, 49:450–457, 1972.

[9] R. MacFarlane and A. Kahler. Methods for processing ENDF/B-VII with NJOY. *Nuclear Data Sheets*, 111:2739–2890, 2010.

[10] R. Macfarlane and D. Muir. The NJOY nuclear data processing system, version 91. Technical Report LA-12740-M, Los Alamos National Laboratory, 1994.

[11] R. E. MacFarlane, R. M. Blomquist, D. E. Cullen, E. Lent, and J. C. Sublet. A code comparison study for the bigten critical assembly. Technical Report LA-UR-08-4668, Los Alamos National Laboratory, 2008.

[12] R. D. Mosteller and R. C. Little. Impact of MCNP unresolved resonance probability-table treatment on uranium and plutonium benchmarks. Technical Report LA-UR-98-2943, Los Alamos National Laboratory, 1998.

[13] NEA Nuclear Science Committee. International handbook of evaluated criticality safety benchmark experiments. Technical Report NEA/NSC/DOC(95)03, OECD Nuclear Energy Agency, 2013.

[14] J. C. Sublet, P. Ribon, and M. Coste-Delclaux. CALENDF-2010: user manual. Technical Report CEA-R-6277, French Alternative Energies and Atomic Energy Commission, 2011.

[15] T. Sutton and F. Brown. Implementation of the probability table method in a continuous-energy Monte Carlo code system. Technical Report KAPL-P-000092, Knolls Atomic Power Laboratory, 1998.

[16] H. R. Trellue, R. C. Little, M. C. White, R. E. MacFarlane, and A. Kahler. ENDF70: a continuous-energy MCNP neutron data library based on ENDF/B-VII.0. *Nuclear Technology*, 168:832–836, 2009.

[17] Tripoli-4 Project Team, 2008. Tripoli-4 user guide. Technical Report CEA-R-6169, French Alternative Energies and Atomic Energy Commission, 2008.

[18] A. Trkov, M. Herman, and D. Brown. ENDF-6 formats manual. Technical Report BNL-90365-2009 Rev.2, National Nuclear Data Center, Brookhaven National Laboratory, 2012.

[19] X-5 Monte Carlo Team. MCNP – a general Monte Carlo n-particle transport code, version 5. Technical Report LA-UR-03-1987, Los Alamos National Laboratory, 2008.